Pergamon

Geochimica et Cosmochimica Acta, Vol. 68, No. 15, pp. 3217–3229, 2004

0016-7037/04 $30.00 + .00

doi:10.1016/j.gca.2003.10.041

Structural constraints of ferric (hydr)oxides on dissimilatory iron reduction and the fate of Fe(II)

COLLEEN M. HANSEL,* SHAWN G. BENNER,† PETER NICO,‡ and SCOTT FENDORF*
Department of Geological and Environmental Sciences, Stanford University, Stanford, CA 94305, USA

(*Received June* 16, 2003; *accepted in revised form October* 28, 2003)

Abstract—Due to the strong reducing capacity of ferrous Fe, the fate of Fe(II) following dissimilatory iron reduction will have a profound bearing on biogeochemical cycles. We have previously observed the rapid and near complete conversion of 2-line ferrihydrite to goethite (minor phase) and magnetite (major phase) under advective flow in an organic carbon-rich artificial groundwater medium. Yet, in many mineralogically mature environments, well-ordered iron (hydr)oxide phases dominate and may therefore control the extent and rate of Fe(III) reduction. Accordingly, here we compare the reducing capacity and Fe(II) sequestration mechanisms of goethite and hematite to 2-line ferrihydrite under advective flow within a medium mimicking that of natural groundwater supplemented with organic carbon. Introduction of dissolved organic carbon upon flow initiation results in the onset of dissimilatory iron reduction of all three Fe phases (2-line ferrihydrite, goethite, and hematite). While the initial surface area normalized rates are similar ($\sim 10^{-11}$ mol Fe(II) m^{-2} g^{-1}), the total amount of Fe(III) reduced over time along with the mechanisms and extent of Fe(II) sequestration differ among the three iron (hydr)oxide substrates. Following 16 d of reaction, the amount of Fe(III) reduced within the ferrihydrite, goethite, and hematite columns is 25, 5, and 1%, respectively. While 83% of the Fe(II) produced in the ferrihydrite system is retained within the solid-phase, merely 17% is retained within both the goethite and hematite columns. Magnetite precipitation is responsible for the majority of Fe(II) sequestration within ferrihydrite, yet magnetite was not detected in either the goethite or hematite systems. Instead, Fe(II) may be sequestered as localized spinel-like (magnetite) domains within surface hydrated layers (ca. 1 nm thick) on goethite and hematite or by electron delocalization within the bulk phase. The decreased solubility of goethite and hematite relative to ferrihydrite, resulting in lower $Fe(III)_{aq}$ and bacterially-generated $Fe(II)_{aq}$ concentrations, may hinder magnetite precipitation beyond mere surface reorganization into nanometer-sized, spinel-like domains. Nevertheless, following an initial, more rapid reduction period, the three Fe (hydr)oxides support similar aqueous ferrous iron concentrations, bacterial populations, and microbial Fe(III) reduction rates. A decline in microbial reduction rates and further Fe(II) retention in the solid-phase correlates with the initial degree of phase disorder (high energy sites). As such, sustained microbial reduction of 2-line ferrihydrite, goethite, and hematite appears to be controlled, in large part, by changes in surface reactivity (energy), which is influenced by microbial reduction and secondary Fe(II) sequestration processes regardless of structural order (crystallinity) and surface area.

1. INTRODUCTION

Iron (hydr)oxides are ubiquitous in the environment with contents ranging from one to several hundred g kg^{-1} in aerobic soils (Cornell and Schwertmann, 1996). The dominant means of iron (hydr)oxide reduction within anaerobic, nonsulfidogenic conditions is by way of bacterial Fe(III) respiration (Lovley et al., 1991). Dissimilatory iron-reducing bacteria couple the oxidation of H_2 or organic carbon to the reduction of Fe(III) with the subsequent generation of energy in the form of adenosine triphosphate (ATP) (Lovley and Phillips, 1988; Lovley, 1991; Nealson and Saffarini, 1994). Dissimilatory iron-reducing bacteria are ubiquitous in subsurface environments being phylogenetically and physiologically diverse (Lovley and Phillips, 1988; Lovley, 1991; Caccavo et al., 1992; Caccavo et al., 1994; Nevin and Lovley, 2000; Childers and Lovley, 2001; Nevin and Lovley, 2002). The genetic system involved in acquisition and reduction of Fe(III) within sparingly soluble iron (hydr)oxides is unresolved and is currently a topic of intense investigation (Gorby and Lovley, 1991; DiChristina and DeLong, 1994; Myers and Myers, 1998; Magnuson et al., 2000; Coppi et al., 2001; DiChristina et al., 2002; Thompson et al., 2002; Leang et al., 2003; Lloyd et al., 2003). The mechanisms of iron reduction are diverse, including extracellular electron transfer requiring direct cell-oxide contact or production of soluble Fe(III) chelators and electron shuttling compounds (e.g., quinones) (Lovley and Woodward, 1996; Nevin and Lovley, 2000; Newman and Kolter, 2000; Childers et al., 2002; Nevin and Lovley, 2002). The particular means of reduction appears to not only vary depending on the species of iron-reducing bacteria, but also as a function of the conditions under which reduction occurs.

A spectrum of iron (hydr)oxides exists in the environment having a diverse range of crystallinities and subsequent reactivities (Cornell and Schwertmann, 1996; Schwertmann and Cornell, 2000). The thermodynamic stability of iron (hydr)oxides is a function of crystal structure and particle size, which ultimately controls the solubility of the (hydr)oxide phases. Solubility of iron (hydr)oxides generally decreases from ferri-

* Authors to whom correspondence should be addressed (hansel@stanford.edu, fendorf@stanford.edu).
† *Present address:* Division of Hydrologic Sciences, Desert Research Institute, Las Vegas, NV 89119, USA.
‡ *Present address:* Department of Chemistry, California State University, Stanislaus, Turlock, CA 95382, USA.

hydrite ($K_{so} = 10^{-39}$) to goethite ($K_{so} = 10^{-41}$) to hematite ($K_{so} = 10^{-43}$) at circumneutral pH (Langmuir, 1969; Baes and Mesmer, 1976; Cornell and Schwertmann, 1996). Depending on the mechanism of dissimilatory reduction, the solubility of the iron (hydr)oxide substrates may impart a constraint on the extent and rate of Fe(III) reduction. Recently, however, the thermodynamic properties (ΔG_r, K_s) of iron (hydr)oxides was found to have only a secondary control on Fe(III) reduction rates by *Shewanella putrefaciens* (CN32) (Roden, 2003). Instead, Fe(III) reduction rates of various Fe (hydr)oxides appear to be correlated with surface area (Roden and Zachara, 1996; Roden, 2003). Given the greater abundance but lower surface area of more crystalline iron (hydr)oxides in the environment, microbial reduction of phases such as goethite and hematite may substantially contribute to the long-term potential for Fe(II) generation, sequestration, and associated biogeochemical cycles. Furthermore, they may undergo intense degradation through reductive dissolution or biotransformation, thus altering the reactive components of a system.

In addition to their importance as terminal electron acceptors, the fate of many nutrients and metals is dictated, in part, by iron (hydr)oxide formation and transformations. For instance, the reductive dissolution of iron (hydr)oxides by dissimilatory iron-reducing bacteria may either enhance (release of sorbed ions) or diminish (reductive immobilization via redox active metabolites) contaminant fate and transport within subsurface environments. Due to the strong reducing capacity of ferrous Fe, the fate of Fe(II) following dissimilatory iron reduction will have a profound bearing on metal cycles, including Cr (Fendorf et al., 2000; Wielinga et al., 2001; Hansel et al., 2003b). Additionally, continued microbial reduction of Fe(III) substrates is impeded by Fe(II) precipitation and complexation to bacterial and/or oxide surfaces (Roden and Urrutia, 1999; Urrutia et al., 1999; Roden and Urrutia, 2002; Royer et al., 2002). The ultimate fate of Fe(II) will, therefore, have a direct and profound bearing on the biogeochemical cycling of Fe and associated nutrients and contaminants. Secondary mineralization pathways of Fe(II) following dissimilatory iron reduction of ferrihydrite are controlled, in large part, by the supply rate and concentration of Fe(II) in solution (Fredrickson et al., 1998; Benner et al., 2002; Zachara et al., 2002; Hansel et al., 2003a). As such, the fate of Fe(II) and subsequent secondary mineralization may substantially differ among iron (hydr)oxides varying in microbial bioavailability.

Iron-reducing bacteria are thought to preferentially utilize poorly-ordered phases, such as ferrihydrite, thus explaining the persistence of more crystalline iron (hydr)oxide phases in the environment (Lovley and Phillips, 1986; Phillips et al., 1993). Yet, in mature environments, well-ordered iron (hydr)oxide phases dominate and may therefore control the extent and rate of Fe(III) reduction. We have previously observed the rapid and near complete conversion of 2-line ferrihydrite to goethite (minor product) and magnetite (major product; $[Fe^{2+}]>0.4$ mM) under advective flow in an artificial groundwater medium supplemented with 3 mM lactate (Benner et al., 2002; Hansel et al., 2003a). The addition of merely 40 μM ferrous Fe to 2-line ferrihydrite results in near complete (90%) conversion to goethite and lepidocrocite within 2 h (Hansel et al., 2003a). As such, the persistence of iron (hydr)oxides in the environment may stem from a microbially generated ferrous Fe-catalzyed Oswald ripening process. Thus, even in relatively young systems, the predominant substrates available for dissimilatory iron reduction may instead be more crystalline (thermodynamically stable) iron (hydr)oxides such as goethite and hematite. Accordingly, here we compare the reducing capacity and Fe(II) sequestration mechanisms of goethite and hematite to 2-line ferrihydrite under advective flow within a medium mimicking that of natural groundwater supplemented with organic carbon.

2. EXPERIMENTAL METHODS AND PROCEDURES

Microbial reduction of 2-line ferrihydrite, goethite, and hematite was investigated using a number of columns performed in two main experimental studies. The first study consisted of a series of 2-line ferrihydrite, goethite, and hematite columns (1 column per oxide) that were reacted for 16 d and the aqueous chemistry and exported cells were monitored daily within both the effluent and side ports. The microbial cell distribution (numbers and surface organization) associated with the solid-phase and secondary mineral phases were determined exclusively at the termination of the experiment following 16 d of reaction. This set of columns is the focus of the results and discussion to follow. A second set of column experiments was performed where 5 smaller columns for each iron (hydr)oxide were run simultaneously and terminated at varying time points. This series of columns was conducted to check for reproducibility, determine the influence of initial Fe(III) concentration, and to observe temporal variation in microbial distribution on the iron (hydr)oxide surfaces. The experimental details for these two studies are provided in the following sections. Experimental conditions and analyses are similar between the two studies unless noted otherwise.

2.1. Preparation of Media and Bacterial Cultures

We examined microbially induced Fe (hydr)oxide reductive dissolution and biomineralization using *Shewanella putrefaciens* strain CN32 in an organic carbon-rich artificial groundwater medium under advective flow. *Shewanella putrefaciens* is a facultative, dissimilatory iron-reducing bacterium (DIRB) that couples the oxidization of lactate to acetate with Fe(III) reduction. Standard methods for culture of anaerobic bacteria and preparation of anoxic media were used throughout. Media and buffers were made anoxic by boiling and cooling under a stream of O_2-free N_2 or N_2:CO_2 (80:20) gas. All reactions were performed in an anaerobic chamber (Coy Laboratories, Inc., Grass Lake, MI) with a N_2 (90%):H_2(10%) atmosphere. *S. putrefaciens* was grown aerobically to late log phase in tryptic soy broth (TSB, DIFCO, Detroit, MI) at room temperature and frozen in 20% glycerol at −80°C. Seed cultures were started from frozen stocks (1 mL in 100 mL TSB) and grown aerobically for 12 h at room temperature (150 rpm). Cell suspensions were prepared by adding 1 mL of the seed culture to 100 mL of TSB and grown to late log phase (12 h, 25°C, 150 rpm). Cells were harvested by centrifugation (4500 *g* 10 min, 5°C), washed twice in 100 mL of bicarbonate buffer (2.5 g $NaHCO_3$ and 2.5 g NaCl per liter, pH 7.0) and resuspended in an artificial groundwater medium. The artificial groundwater medium contained the following ingredients (in mg/L): NaCl, 30; NH_4Cl, 0.95; KCl, 5; $MgSO_4$, 50; KH_2PO_4, 0.95 and 1 mL mineral solution (Balch et al., 1979) (Table 1). Lactate (as sodium lactate) was added as the electron donor to give a final concentration of ~3 mM. The medium was equilibrated and maintained (within an enclosed bottle) at equilibrium with calcite (0.4 g/L) and an atmosphere of 2% CO_2/98% N_2 (pH=7). Batch studies indicate that the groundwater medium supports microbial growth (Hansel et al., 2003a).

Two-line ferrihydrite-, goethite-, and hematite-coated quartz sand were prepared by first producing a slurry of each phase. Ferrihydrite was prepared by titrating a ferric chloride solution with NaOH to a pH of 7.5. The titration was conducted rapidly (less than 5 min) to avoid precipitation of akaganeite. High surface area goethite was prepared by slow oxidation of a ferrous chloride/sodium bicarbonate solution (Schwertmann and Cornell, 2000). Hematite was made by slow titration of a ferric nitrate solution to boiling DI water (Schwertmann and Cornell, 2000). After washing the Fe oxide flocs by either centrifugation or dialysis, quartz sand was added to the suspension. Excess water

Table 1. Average feed solution chemistry.

Element	mM	SD
Ca	2.9	0.4
Fe	0	0
K	0.09	0.02
Mg	0.42	0.03
Na	1.3	0.6
P	0.007	0.003
S	0.43	0.01
Si	0.04	0.02
Cl	0.08	0.01
lactate	3.2	0.7
NH_4Cl	0.02	—
pH	7	0.3
alkalinity	2.8 mEq	0.5
Wolfe's mineral solution	0.1 mL/L	—

was decanted and the remaining solution and sand allowed to evaporate at 20°C under convection while the mixture was periodically stirred. The coated sand was dried at 20°C for 4 d and then resaturated with water and heat sterilized. Both X-ray diffraction (XRD) and X-ray absorption spectroscopy (XAS) verified the Fe (hydr)oxide phases. No change in mineralogical composition (XAS and XRD) or surface area (BET analysis) was noted following sterilization of the Fe (hydr)oxide-coated sands. Surface area analysis was conducted on a Beckman-Coulter SA3100 analyzer using a single-point isotherm with N_2(g) as the adsorbate on He (24 h) purged samples. The surface area of the Si sand was found to be negligible in comparison to the (hydr)oxide-coated sands. Freshly precipitated Fe (hydr)oxide-coated sand was inoculated with *S. putrefaciens* to a cell density of 5×10^8 cells g^{-1} before loading the columns.

2.2. Column Design and Flow Conditions

Experiments were conducted using 3 columns having a 3.8 cm (inner) diameter and a 25 cm length; solution sampling ports were located every 2.5 cm along the length of the column. Inoculated Fe (hydr)oxide-coated sand (saturated with media) was added under continuous vibration to obtain a uniform packing (continuous bulk density of 1.39 g/cm^3) and allowed to equilibrate for 1 h before initiating flow. Flow velocities upward through the column were maintained at ~1.6 pore volumes per day, equivalent to a pore water velocity of approximately 40 cm d^{-1}.

Additional experiments were conducted using a series of 4 columns for each iron (hydr)oxide (12 columns in total), which were terminated at 4 different time points to investigate microbial surface colonization over time and check for reproducibility of the previous column results. The columns were constructed of glass having a 8.2 cm length and 1.5 cm diameter, containing only influent and effluent ports. The smaller columns had an equivalent pore water residence time as that in the larger column set. Due to the difficulty in microscopic imaging of uneven surfaces, iron (hydr)oxides were coated onto etched glass rods having a rectangular cross section (3 mm × 5 mm × 5 cm). Rods containing a coating corresponding to the Fe (hydr)oxide coated sand were inserted down the center of each column during loading. All experiments were conducted in an anaerobic glove bag.

2.3. Sampling and Analyses

All columns were connected to a communal pump and feed solution to minimize induced (artificial) heterogeneity. Upon termination, the solids were carefully extracted and homogenized at 2 cm intervals along the length of the column. Solids intended for X-ray absorption spectroscopic analyses were dried unaltered in the anaerobic glovebox, mounted on a Teflon plate, and sealed with Kapton polymide film to prevent moisture loss and oxidation while minimizing X-ray adsorption. Reproducibility of the bacterial, solution, and solid-phase results were tested by comparison among columns for overlapping time periods. Bacterial, solution, and solid-phase analyses were conducted as described in the following subsections.

2.3.1. Bacteria

Viable bacteria eluting from the column were quantified by serial dilution, plating on tryptic soy agar, and incubating the plates under aerobic conditions. Bacteria associated with the solid-phase were also enumerated and checked for purity at the conclusion of the column experiments using plate counts. A 1 g sample of iron-coated sand was added to 9 mL of 0.01 mol/L sodium pyrophosphate and subjected to low-level sonication before serial dilution and plating.

The temporal distribution of bacteria on the mineral surfaces was investigated using epifluorescence microscopy for the smaller set of time series columns. Upon termination, the glass columns were split in half and the sand carefully removed from the Fe (hydr)oxide-coated rod surface. Iron (hydr)oxide-coated sand and rods were immediately fixed upon column termination by addition of 3 volumes of freshly prepared 4% paraformaldehyde/phosphate buffered saline (PBS) solution and incubated at 4°C for 3 h. Samples were rinsed and resuspended in a PBS/96% ethanol solution (1:1, v/v) and stored at 4°C. To avoid nonselective staining, bacteria were visualized by fluorescent in situ hybridization (FISH) using a Bacteria probe (EUB338) as described previously (Bond and Banfield, 2001). Fixed samples (Fe oxide-coated sand and rods) were dried and then dehydrated by immersing the samples for 3 min into a series of 50, 80, and 90% ethanol solutions. Samples were hybridized in buffer (0.9 mol/L NaCl, 20 mM Tris/HCl, pH 7.4, 0.01% sodium dodecyl sulfate) containing 25–50 ng of EUB338 probe and 20% formamide for 2 h at 46°C in an equilibrated humidity chamber. Samples were then rinsed and soaked in wash buffer (20 mM Tris/HCl, pH 7.4, 0.01% SDS, and 0.23 mol/L NaCl) for 15 min. at 48°C. Lastly, the samples were rinsed and viewed using a Nikon epifluorescent microscope.

2.3.2. Solution

Solution from the feed, effluent, and side sampling ports were obtained for major dissolved constituents and pH as a function of time. Production of soluble Fe(II) was monitored spectrophotometrically at 562 nm using the ferrozine assay (Stookey, 1970). Total dissolved Fe and other major ions (Ca, K, Mg, P, Si, Na) were determined by inductively coupled plasma optical emission spectroscopy (ICP-OES). Acetate and lactate concentrations were obtained using ion chromatography (IC).

2.3.3. Solid Phase

2.3.3.1. Extractions. Solid-phase extractions were performed by adding either 1 mL of 0.5 mol/L (partial extraction) or 6 mol/L (total extraction) HCl to 1 g of sample and shaking for 3 to 8 h. The supernatant was filtered, diluted with DI water and analyzed via ICP-OES for total Fe and colorimetric assays for Fe(II). Within the ferrihydrite columns, the concentration of Fe(II) within the extracts was determined with the ferrozine assay for Fe(II) (discussed above). The ferrozine assay, however, is inaccurate for systems having low Fe(II) concentrations, specifically within a high Fe(III) matrix. A modified Fe(II) assay using 1,10-phenanthroline and fluoride as an Fe(III) masking agent was used for the goethite and hematite extracts (Tamura et al., 1974; Jeon et al., 2001).

2.3.3.2. Spectroscopy. The speciation and structural environment of Fe were determined using X-ray absorption spectroscopy (XAS). XAS analyses were conducted on beamline 4–1 and 4–3 (8 pole wiggler) at the Stanford Synchrotron Radiation Laboratory (SSRL), running under dedicated conditions. Spectra acquisition and analyses was conducted as described in detail previously (Benner et al., 2002; Hansel et al., 2003a). Briefly, extended X-ray absorption fine structure (EXAFS) spectra were collected from −200 to +1000 eV about the K-edge of Fe. Each scan was calibrated internally by placing an iron metal foil between the second and third in-line ionization chambers and setting the first inflection point of Fe^0 to 7111.0 eV. A set of reference standards for Fe, including siderite ($FeCO_3$), 2- and 6-line ferrihydrite ($Fe(OH)_3 \cdot nH_2O$), goethite (α-FeOOH), lepidocrocite (γ-FeOOH), hematite (α-Fe_2O_3), green rust ($Fe^{II}_{6-x}Fe^{III}_x(OH)_{12}[(SO_4)_{x/2} \cdot 3H_2O]$),

iron sulfide (FeS), vivianite [$Fe_3(PO_4)_2 \cdot nH_2O$], and magnetite (Fe_3O_4) (for more details, see Hansel et al., 2003a), was utilized to perform linear combination k^3-weighted EXAFS spectral fitting using the EXAFSPAK module DATFIT (George, 1993). Linear fitting routines were used to reconstruct the unknown to determine the relative percentages of mineral phases within the samples. Linear combinations of empirical model spectra were optimized where the only adjustable parameters were the fractions of each model compound contributing to the fit. Fits were optimized by minimizing the residual, defined as the normalized root square difference between the data and the fit. The accuracy of qualitative and quantitative results of linear combination Fe EXAFS fits was investigated using Mössbauer spectroscopy and also fitting a set of mixed standards having known fractions (Hansel et al., 2003a). Fits were within ±5% of the actual mole percentages using the k-range 1–14 $Å^{-1}$. The detection limit for minor constituents was ~5%.

2.3.3.3. Microscopy. Iron (hydr)oxide phase surface alteration and phase transformations were investigated via high resolution transmission electron microscopy (HRTEM). Reacted iron-(hydr)oxide coated sand was directly applied and dried onto a carbon-coated Cu grid with a formvar support film in an anaerobic glovebox. Imaging and analyses were performed using a JEOL 2010 high-resolution TEM, which was equipped with a LaB6 filament as an electron source and operated at 200 kV, with 1.9 resolution. Images were digitally collected and analyzed using Digital Micrograph software (Gatan, Inc.). For elemental analysis, an Oxford Link ISIS X-ray EDS microanalysis system was coupled to the TEM. Selected area electron-diffraction ring patterns were collected from nanocrystalline material, and evaluated by Desktop Microscopist (Lacuna Labs) software. The nominal accuracy of the d-spacings is ~0.1 nm.

3. RESULTS AND DISCUSSION

As described above, a series of column experiments were conducted within two main study venues. In brief, the first study consisted of a series of 2-line ferrihydrite, goethite, and hematite columns that were reacted for 16 d and the aqueous chemistry and exported viable cells were monitored daily within both the effluent and side ports. The microbial cell distribution (numbers and surface organization) associated with the solid-phase and secondary mineral phases were determined only at the termination of the experiment following 16 d. This set of columns is referred to as the "16 d reacted" columns and is the primary focus of the results and discussion to follow. A second set of column experiments was performed where 5 smaller columns for each iron (hydr)oxide (15 columns in total) were run simultaneously and terminated at varying time points. This series of columns was conducted to check for reproducibility, to determine the influence of initial Fe(III) loading, and to observe microbial distribution on the iron (hydr)oxide surfaces as a function of time. In the following text, these columns will be referred to as the "time series" columns.

3.1. Evidence of Fe(III) Reduction

Initiation of flow and subsequent introduction of dissolved organic carbon results in Fe(II) generation within the 2-line ferrihydrite, goethite, and hematite columns (Fig. 1a); Fe(II) is eluted from the ferrihydrite and goethite columns at equivalent concentrations for the first 2 pore volumes but is absent in the hematite column effluent for more than 3 pore volumes. Peak ferrous Fe concentrations are 5× higher for ferrihydrite (1.0 mM) than for both goethite and hematite (0.2 mM). Coinciding with the initiation of Fe(III) reduction, effluent Eh values vary between 25 and 50 mV for the 3 columns and the pH of the effluent waters in the ferrihydrite column initially decrease but increase for goethite and hematite (Fig. 1b). The pH values

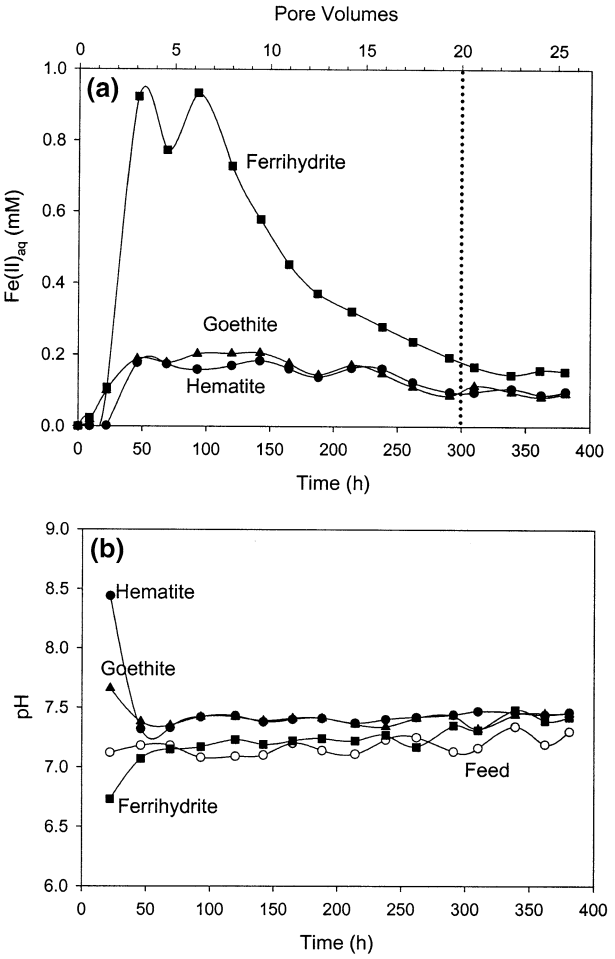

Fig. 1. (a) Effluent concentrations of Fe(II) throughout the course of the experiment (16 d) for the three different Fe (hydr)oxide columns. Dotted line represents time approaching pseudo–steady-state conditions. (b) Effluent pH values as a function of time.

after 1 d range from 6.8 to 7.7 to 8.5 for ferrihydrite, goethite, and hematite, respectively. The observed Fe(II) profiles and progression of pH values likely results from the interplay of adsorption reactions of Fe(II) (represented by reaction 2) offsetting proton consumption from respiration-driven Fe(III) reduction (reaction 1).

$$4Fe(OH)_3 + CH_3CHOHCOO^- + 7H^+ \leftrightarrow 4Fe^{2+} + CH_3COO^- + HCO_3^- + 10H_2O \quad (1)$$

$$\equiv Fe—OH + Fe^{2+} \leftrightarrow \equiv Fe—OFe^{2+} + H^+ \quad (2)$$

The generation of ferrous Fe within the columns corresponds with the production of acetate (Fig. 2). Peak acetate concentrations are approximately 3 mM for ferrihydrite, 650 μM for goethite, and 450 μM for hematite. Within the three columns, near-linear temporal profiles of acetate, as revealed by the side-port data, are observed, indicating uniform generation throughout the column (data not shown). Additionally, within all 3 columns, a ferrous Fe pulse is present following 1 d of reaction (Fig. 3). Ferrous Fe profiles between 3 and 9 d are

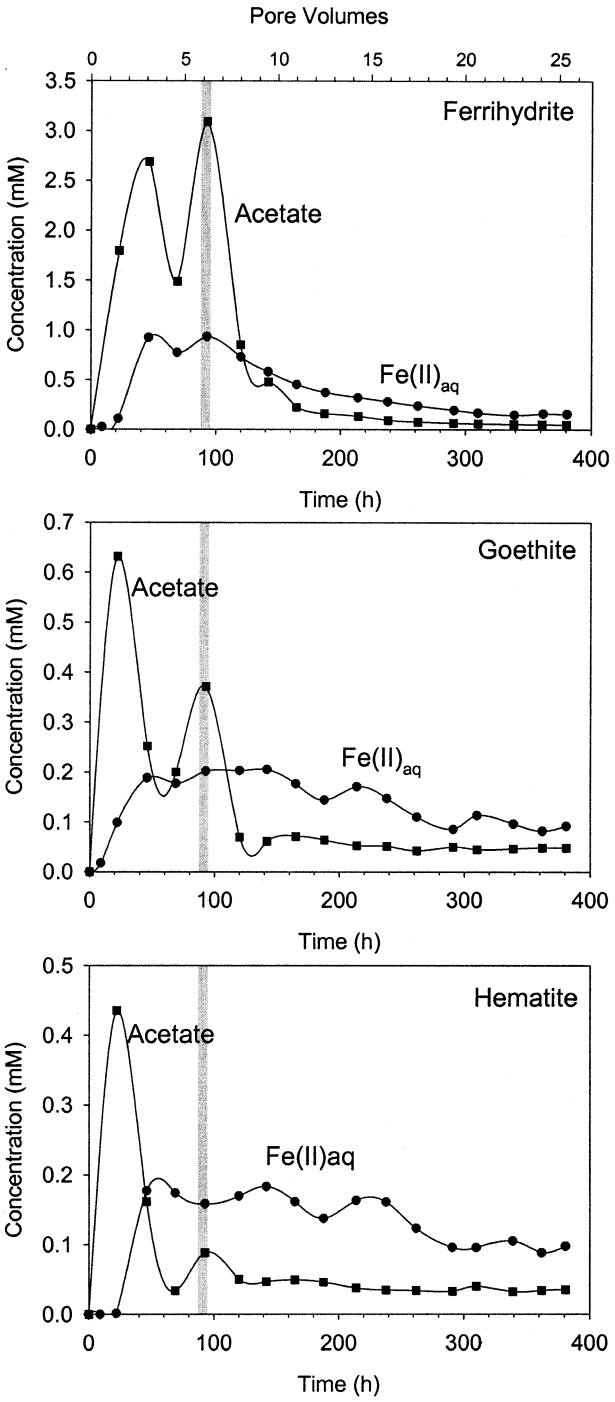

Fig. 2. Effluent concentrations of acetate and Fe(II) for each ferric (hydr)oxide. Shaded gray box indicates time period (~90 h) where flow was interrupted for 8 h, represented by a second acetate pulse in the effluent at ~100 h.

linear for goethite and hematite suggesting uniform Fe(II) retention along the length of the column. In contrast, Fe(II) profiles within the ferrihydrite column have an abrupt change at ~5 cm from the inflow, indicating a higher degree of Fe(II) retention downgradient, as observed previously (Hansel et al., 2003a).

There are conflicting reports on the reduction of crystalline ferric (hydr)oxides such as goethite. The reduction of goethite via dissimilatory iron reduction is well-documented under both static and dynamic flow, nutrient-rich conditions (Roden and Zachara, 1996; Roden et al., 2000; Liu et al., 2001; Roden, 2003). Recently, however, reduction of goethite by *S. putrefaciens* (CN32) was not observed under static, less nutrient-rich conditions (Glasauer et al., 2003). In the present study, microbial iron respiration coupled to incomplete lactate oxidation within ferrihydrite, goethite, and hematite columns occurs under advective flow in a medium (Table 1) and flow rate (40 cm d^{-1}) typical of organic carbon-rich natural groundwater systems (Figs. 1–3). Reduction is maintained within each system for the entirety of the experiment (16 d); we also observe continued reduction beyond 43 d for the time series columns. Despite the lean (minimal) media used in these experiments, reduction of the crystalline iron (hydr)oxides goethite and hematite is observed.

The initial stage of reduction (<200 h) of goethite and hematite is substantially different from that of ferrihydrite. Over the first 200 h, 2.5 mmol of acetate are generated in the ferrihydrite column in contrast to 0.32 and 0.14 mmol in the goethite and hematite systems, respectively. Yet, while the absolute rates of Fe(III) reduction (mol Fe(II) s^{-1}) differ, initial surface area normalized Fe(III) reduction rates are equivalent (~10^{-11} mol Fe(II) m^{-2} g^{-1}) (Table 2)—rates consistent with previous studies (Benner et al., 2002; Hansel et al., 2003a) and trends in agreement with surface area as a dominant control on the microbial reduction of iron (hydr)oxides (Roden and Zachara, 1996; Roden, 2003). As mentioned previously, the time series columns contain an equivalent quantity of Fe(III) initially to determine its impact on the extent of Fe reduction and reduction rates. The initial Fe(III) content does not change the previously observed reduction rates nor extent of reduction, which are again equivalent when normalized to surface area.

3.2. Fe(II) Sinks and Impact on Secondary Mineralization

Acid extractions of the column solids disclose the distribution of ferrous and ferric iron within the solid-phase (Fig. 4). Average Fe(III) content within the ferrihydrite and hematite columns are ~10 mg g^{-1} (Fig. 4). In an attempt to equate the available Fe oxide surface area within the goethite and hematite columns, the average solid-phase Fe(III) content within the goethite column (~3 mg g^{-1}) is approximately one-third that in the hematite column. The corresponding surface area of the oxide-coated sands within the ferrihydrite, goethite, and hematite columns is 3, 0.4, and 0.5 m^2 g^{-1}, respectively. Following 16 d of reaction, variable Fe contents, and hence degrees of Fe transfer, are evident among the 3 (hydr)oxide columns (Fig. 4). Within the ferrihydrite column, a decline in Fe content occurs within the first 5 cm along the flow path. In contrast, transport of Fe occurs over the length of both the goethite and hematite columns.

Deviation from the 4:1 stoichiometry between ferrous Fe and acetate (reaction 1) for all the iron (hydr)oxide columns (Figs. 2 and 3) coupled with Fe(II) speciation data from solid-phase extracts (Fig. 4), indicates that Fe(II) is being retained in the solid-phase. Goethite and hematite illustrate a similar control

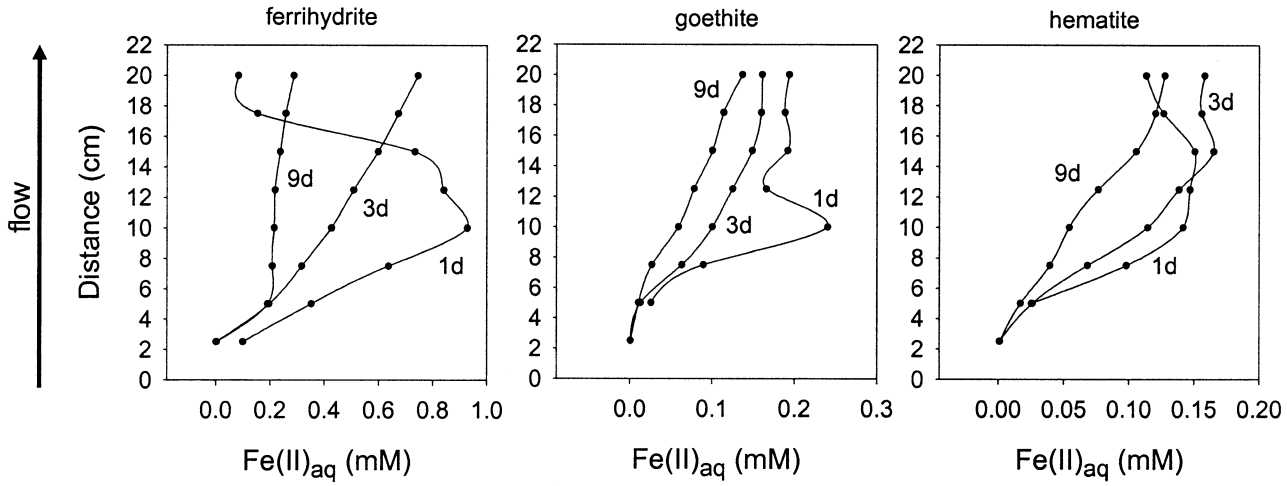

Fig. 3. Iron(II) concentrations along the length of the three Fe (hydr)oxide columns. Numbers adjacent to plots reflect day of sampling.

on the fate of Fe(II), which differs appreciably from that within the ferrihydrite column. The amount of solid-phase Fe(II) in the goethite and hematite columns is equivalent (~0.025 mg g^{-1}), yet levels are 100× higher within the ferrihydrite column (2.4 mg g^{-1}) (Fig. 4). The amount of solid-phase-bound Fe(II) is relatively uniform throughout the columns except for the up-gradient 5 cm in the ferrihydrite column. While 83% of the Fe(II) produced in the ferrihydrite system is retained within the solid-phase, merely 17% is retained within both the goethite and hematite columns (Table 2).

Despite the apparent supersaturated conditions with respect to a suite of ferrous/ferric-bearing minerals (calculated using the geochemical modeling program MINTEQ (Allison et al., 1990) and solubility constants as in Hansel et al., 2003a) for the ferrihydrite, goethite, and hematite effluent waters, only two secondary mineral phases were detected by linear-combination EXAFS analysis. Consistent with previous findings, reductive dissolution of 2-line ferrihydrite results in the secondary precipitation of dominantly (~10–50%) magnetite with lesser (~10%) amounts of goethite (Fig. 5; Benner et al., 2002; Hansel et al., 2003a). The concentration of magnetite increases along the flow path, with average concentrations within the

Table 2. Iron dynamics as a function of initial Fe oxide substrate.[a]

	Ferrihydrite	Goethite	Hematite
Fe(III)			
Initially available (mmol)	46	14	42
Remaining in column (mmol)	34	13	41
Reduced (%)	25	4.6	1.4
As secondary precipitates[b] (mmol)	13	nd	nd
Fe(II)			
Produced (mmol)	12	0.64	0.58
Eluted from column (mmol)	1.6	0.53	0.48
Sequestered in solid-phase (mmol)	10	0.11	0.10
% associated with solid-phase	83	17	17
As secondary precipitates[b] (mmol)	6	nd	nd
Fe(III) reduction rates (μmol Fe(II) h^{-1})			
Initial[c]	55	21	13
Steady state[d]	2.3	1.9	1.3
Fe(III) reduction rates (mol Fe(II) m^{-2} s^{-1})			
Initial[c]	4E-11	6E-11	3E-11
Steady state[d]	9E-13	5E-12	3E-12
Time to reduce remaining Fe(III) (d)[e]	630	291	1279
Surface area (m^2 g^{-1})			
Fe oxide slurry	361	157	57
Fe oxide-coated sand (initial)	2.9	0.40	0.53

[a] nd = not detected.
[b] As mol% Fe determined from EXAFS linear combination fits.
[c] Calculated using initial acetate production profiles and acetate to Fe stoichiometery.
[d] Calculated using acetate generation profiles for time period following 300 h.
[e] Determined using steady-state acetate generation profiles and residual Fe(III).

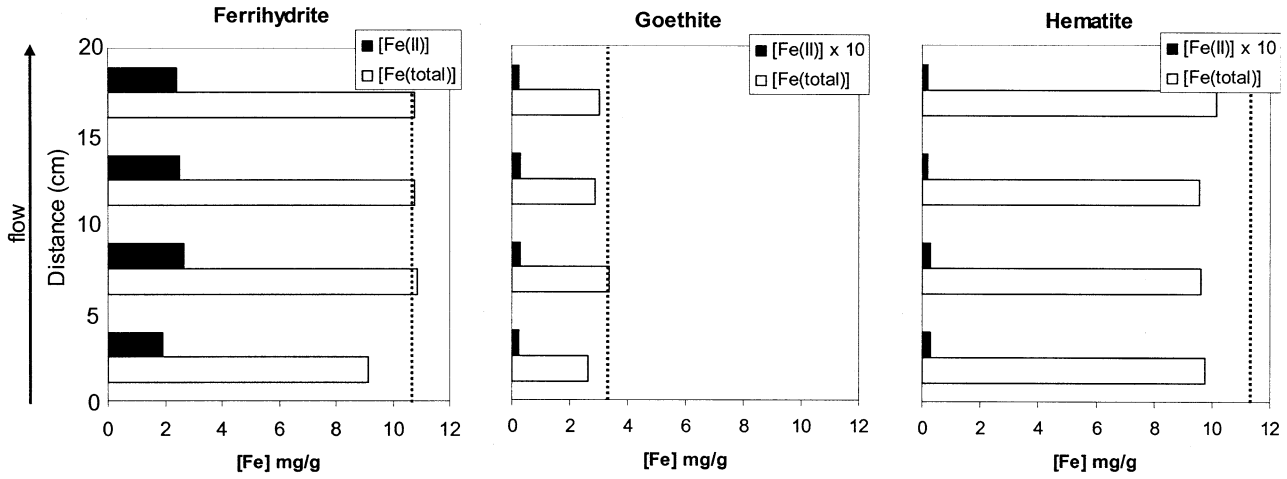

Fig. 4. Concentrations of Fe(II) and total Fe in the solid-phase along the column flow path determined by 6 mol/L HCl extraction. Dotted lines correspond with initial total Fe concentrations within the 3 columns.

upgradient 5 cm section being 10% in comparison to 52% downgradient. Magnetite, therefore, serves as a dominant control in the sequestration of Fe(II) within the column; 60% of the total Fe(II) and 38% of the Fe(III) within the solid-phase are retained within magnetite. The remaining portion of solid-phase bound Fe(II) largely exists as sorption complexes to either the bacterial or mineral surfaces. We have observed previously, however, the existence of green rust in trace quantities (~1%) following reductive dissolution of 2-line ferrihydrite under similar conditions (Hansel et al., 2003a). While the incidence of such trace phases is below linear-combination EXAFS detection limits (~5%) and therefore cannot be eliminated, they would constitute a diminutive fraction of the total Fe(II) mass balance on ferrihydrite in these experiments.

In contrast to ferrihydrite, a secondary precipitate is not detected by linear-combination EXAFS upon reductive dissolution of goethite or hematite. Notwithstanding the absence of detectable secondary phase precipitation, structural alteration of the initial (unreacted) goethite and hematite phases is present. X-ray diffraction analyses of the initial goethite and hematite phases reveal peak broadening suggesting a degree of structural disorder (data not shown). Furthermore, linear-combination EXAFS fits of initial goethite and hematite phases include a measurable component of 2-line ferrihydrite (29 and 6%, respectively) (Fig. 6). It is important to keep in mind, however, that the inclusion of 2-line ferrihydrite in the fitting regime does not denote the presence of a purely ferrihydrite component but instead may simply represent a structural disorder within the solid. Following 16 d of reaction, the component of 2-line ferrihydrite required to adequately reconstruct the experimental EXAFS spectra increases to 34% for both goethite and hematite (Fig. 6). Conventional shell-by-shell fitting of the EXAFS spectra revealed no change in the local order of

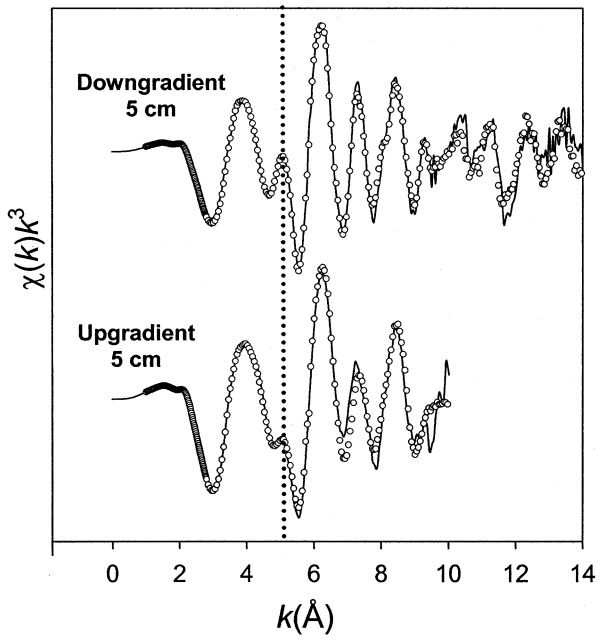

Fig. 5. k^3-weighted EXAFS spectra (solid line) and linear-combination fit (circles) for the solid-phase products in the bottom 5 cm (inflow) and top 5 cm (outflow) from the ferrihydrite column following 16 d of reaction. Vertical dotted line specifies an EXAFS oscillation indicative of the proportion of magnetite.

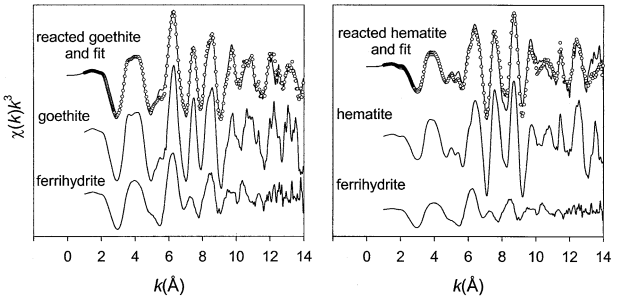

Fig. 6. k^3-weighted EXAFS spectra (solid line) and linear-combination fit (circles) for the solid-phase products from the goethite and hematite columns following 16 d of reaction. Standard spectral components comprised in fits are depicted below the fit experimental spectra. All percents are ±5% and the detection limit is ~5%.

the reacted solids relative to the original goethite and hematite phases (data not shown).

Absence of detectable secondary precipitates suggests that Fe(II) sequestered within goethite and hematite happens largely as sorption complexes to the (hydr)oxide and/or bacterial surfaces. However, addition of 0.5 N HCl, targeted at removing mainly weakly adsorbed Fe(II), did not extract all of the Fe(II) associated with the goethite and hematite solid-phase (total Fe(II) determined via 6 N HCl extraction), suggesting Fe(II) sequestration mechanisms beyond adsorption. A number of studies have identified the inefficiency of 0.5 N HCl in completely extracting ferrous Fe following reaction with varying oxyhydroxides (Tronc et al., 1992; Coughlin and Stone, 1995; Fredrickson et al., 1998; Cooper et al., 2000; Jeon et al., 2001). This inefficiency has been attributed to the failure of 0.5 N HCl in extracting crystalline Fe(II) precipitates (e.g., magnetite) and/or strongly adsorbed Fe(II) species (Tronc et al., 1992; Coughlin and Stone, 1995; Fredrickson et al., 1998; Jeon et al., 2001). Incomplete extraction of Fe(II) was previously noted after reaction with hematite above pH 6 (Jeon et al., 2001). Conversely, complete extraction occurred after Fe(II) reaction at pH values below 6. The authors infer auto-catalytic formation of magnetite, the stability of which is greater than that of hematite above pH 5.9 (Jeon et al., 2001). Recently, however, Mössbauer analysis of isotopic labeled iron (hydr)oxides indicates oxidation of Fe(II) at the surface and subsequent delocalization of electron density within the bulk solid-phase (Scherer, personal communication) consistent with nonlocal electron transfer to hematite by dissimilatory iron-reducing bacteria (Rosso et al., 2003). Either or both of these mechanisms may be operative within this study. Alternatively, yet less likely, Fe(II) may be located within site vacancies or structural defects of the ferric minerals (Coughlin and Stone, 1995).

The heterogeneous precipitation of magnetite from (hydr)oxides may proceed via two means, depending on the (hydr)oxide in question. The precipitation of magnetite in the presence of ferrihydrite occurs via a solid-state conversion driven by Fe(II) adsorption (Cornell, 1988; Tronc et al., 1992; Fredrickson et al., 1998; Zachara et al., 2002; Hansel et al., 2003a). Similarly, for more crystalline iron (hydr)oxides, precipitation of magnetite may be preceded by a hydrated surface layer on the substrate (hydr)oxide leading to nano-scale disordered regions (e.g., ferrihydrite) with subsequent solid-state conversion to magnetite upon reacting with Fe(II). For example, chemisorption (mainly at defect sites) of water on hematite occurs at much lower pressures than that calculated for the conversion of hematite to FeOOH or $Fe(OH)_3$ (e.g., ferrihydrite), the result of which may be from nano-scale Fe(III) hydroxide particles (islands) similar to ferrihydrite on the hematite surface (Liu et al., 1998). Alternatively, the precipitation of magnetite may occur via direct heterogeneous nucleation (e.g., epitaxial growth), such as on the hematite(0001) surface which is crystallographically similar to magnetite(111) (Condon et al., 1998). Both of these processes may be manifested in the EXAFS spectra as an increase in phase disorder from the original crystalline iron (hydr)oxide represented by an enhanced ferrihydrite component in the linear-combination fits.

The formation of surface hydration layers on both goethite and hematite is confirmed using high resolution transmission electron microscopy (Fig. 7). Analysis of lattice fringes reveals a termination of bulk crystalline order at the surface of the grains. Surface associated phase disorder is evident by an approximately 1 nm thick rind on the goethite and hematite particles having no definitive lattice fringes. However, atomic reorganization into spinel domains or discrete sites of magnetite nucleation were also not observed within the hydrated layer. Confirmation of small quantities of magnetite on the (hydr)oxide surfaces may not be feasible due to the small percentage of total Fe (<1%) and small (subnanometer) crystalline domains. We have previously observed ~5-nm-sized magnetite domains throughout ferrihydrite, accompanied by larger magnetite crystals (Hansel et al., 2003a). We postulated that the accumulation of magnetite may depend on both the concentration of Fe(II) and Fe(III) in solution to obtain crystal growth following initial magnetite nucleation (Hansel et el., 2003a). The higher solubility of ferrihydrite may allow for enhanced aqueous Fe(III) concentrations and subsequent magnetite crystal growth, not permitted in the goethite and hematite systems resulting in magnetite-like phase concentrations below EXAFS detection limits and microscopic visualization. Accordingly, lower bacterially-generated Fe(II) concentrations and solubility of goethite and hematite may hinder magnetite precipitation beyond mere surface reorganization into nanometer-sized, spinel-like domains.

3.3. Dissimilatory Fe(III) Reduction

3.3.1. Extent of Reduction

The amount of Fe(III) reduced differs between the three iron (hydr)oxide substrates. Following 16 d of reaction, the amount of Fe(III) reduced within the ferrihydrite, goethite, and hematite columns is 25, 5, and 1%, respectively (Table 2), a trend consistent among systems normalized to both total available Fe(III) (~10 mg g^{-1}) and available surface area for the goethite- (0.4 m^2 g^{-1}) and hematite-coated (0.5 m^2 g^{-1}) sand. A similar trend was noted in batch studies (Roden and Zachara, 1996), with the cessation of microbial reduction attributed to Fe(II) complexation/precipitation on bacterial and/or oxide surfaces. However, while reduction within hydrologically static systems ceases before complete Fe(III) removal, reduction in the present study continues unabated under advective flow due to the removal of Fe(II) and other metabolic end-products. Similarly, enhanced reduction of ferrihydrite, goethite, and hematite within static systems is observed in the presence of Fe(II) complexants and/or electron shuttling compounds (Urrutia et al., 1999; Roden and Urrutia, 2002; Royer et al., 2002). Furthermore, reduction of high surface area goethite in continuous-flow reactors (flow rate of 100 cm d^{-1}) enhances the amount of goethite reduced from 13% in batch to 95% over a 6-mo incubation period (Roden et al., 2000). Assuming continued steady-state reduction rates, it would take approximately 630, 291, and 1279 d for complete reduction of the remaining Fe(III) in the ferrihydrite, goethite, and hematite columns, respectively (Table 2). The shorter time period for goethite relative to ferrihydrite is a consequence of a lower initial Fe(III) loading. Considering an initial Fe(III) content within the goethite column equivalent to ferrihydrite and hematite, it would require ~900 d to reduce the remaining goethite.

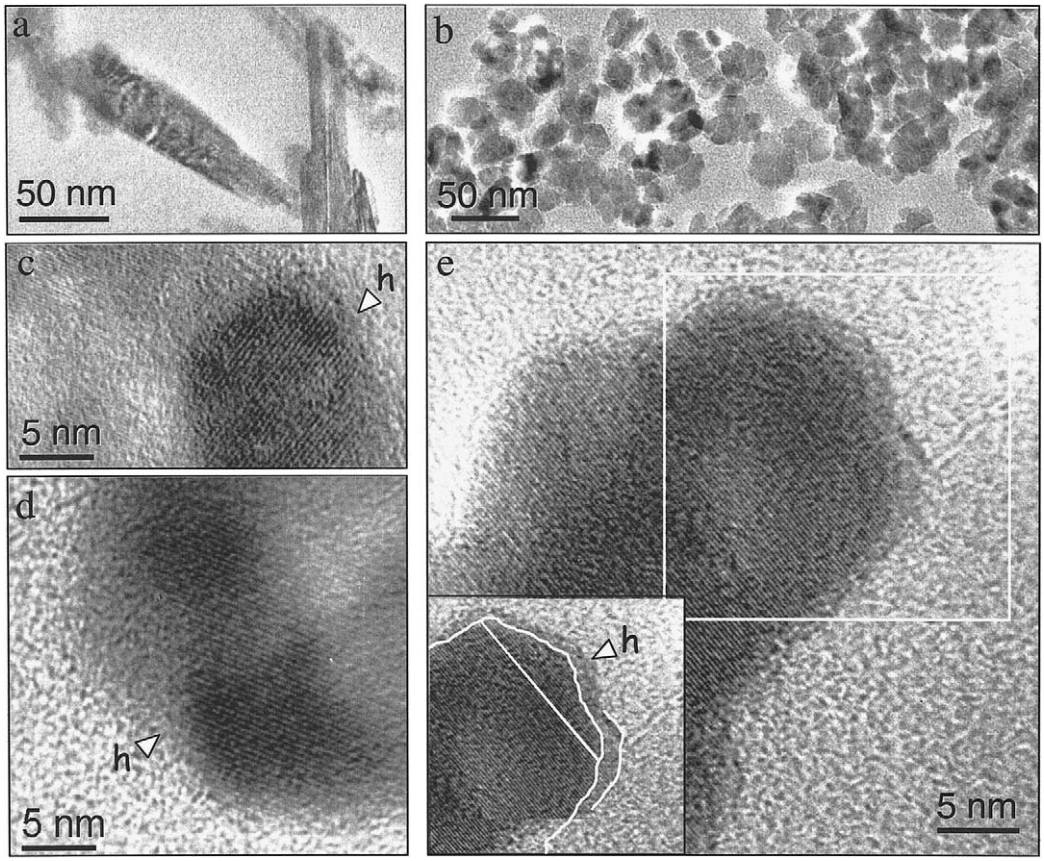

Fig. 7. Transmission electron micrographs illustrating bulk (a) goethite and (b) hematite morphology. Images of lattice fringes reveal the presence of surface hydration layers (arrows with 'h' designation) on both (c) goethite and (d–e) hematite phases following 16 d of reaction. Inset of image (e) illustrates the orientation and termination of *d*-spacings within the bulk hematite precipitate and the ~1 nm thick hydrated (disordered) rind on the grain surface.

The ratio of electron donor to acceptor has previously been identified as an important factor dictating the rate and extent of bacterial reduction of ferrihydrite within batch systems (Fredrickson et al., 2003). The rate and amount of Fe(III) reduction is inversely related to the concentration of ferrihydrite (electron acceptor) relative to lactate (electron donor). The concentration of ferrihydrite, goethite, and hematite within the columns is 317, 99, and 176 mM, respectively (concentration of goethite is lower such that the available surface area is equivalent to hematite; concentration of Fe(III) for ferrihydrite and hematite are equal—2 mol of Fe(III)/mole of hematite as opposed to 1 mol Fe(III) for ferrihydrite and goethite). Considering that the lactate concentration is ~3 mM and a 1:4 stoichiometry for lactate to Fe(III) consumption, the electron donor (lactate) is the limiting substrate (Fe(III) is in excess). However, we do not observe complete consumption of lactate along the length of the columns, suggesting that either maximum bacterial rates are obtained or, most likely, that a decrease in readily available (accessible) Fe(III) limits lactate consumption. Additionally, the rate (~30 μmol h^{-1}) and extent (25%) of ferrihydrite reduction are representative of a higher donor to acceptor ratio according to previous observations within batch systems (Fredrickson et al., 2003). The higher rate and extent of reduction is most likely a consequence of solute transport (via advective flow) within the columns thus minimizing Fe(II) (or other products) adsorption onto bacterial cell surfaces and subsequent inhibition of enzymatic Fe(III) reduction activity.

3.3.2. *Steady-State Fe(III) Reduction*

Goethite reduction by *S. putrefaciens* has a first-order kinetic dependence on surface site availability, which is a function of Fe(II) adsorption and secondary precipitation (Liu et al., 2001). As mentioned in the previous section, advective flow would diminish the aforementioned constraints through the removal of soluble species allowing for decreased retention via adsorption/precipitation (Liu et al., 2001). Correspondingly, we observe continued, unabated reduction of iron (hydr)oxides under advective flow, yet the rate of reduction decreases an order of magnitude following approximately 300 h of reaction—the time at which all three (hydr)oxide phases appear to approach a pseudo–steady state.

While the initial conditions of reduction and Fe(II) retention differ between the ferrihydrite and goethite/hematite systems, the aqueous chemistry and microbial dynamics of the three systems converge following approximately 300 h of reaction for both the 16 d reacted and the time-series columns (43 d). Given an open system, a kinetically-driven equilibrium between the reduction, retention, and transport rates results in a steady-state within the three (hydr)oxide columns. Following

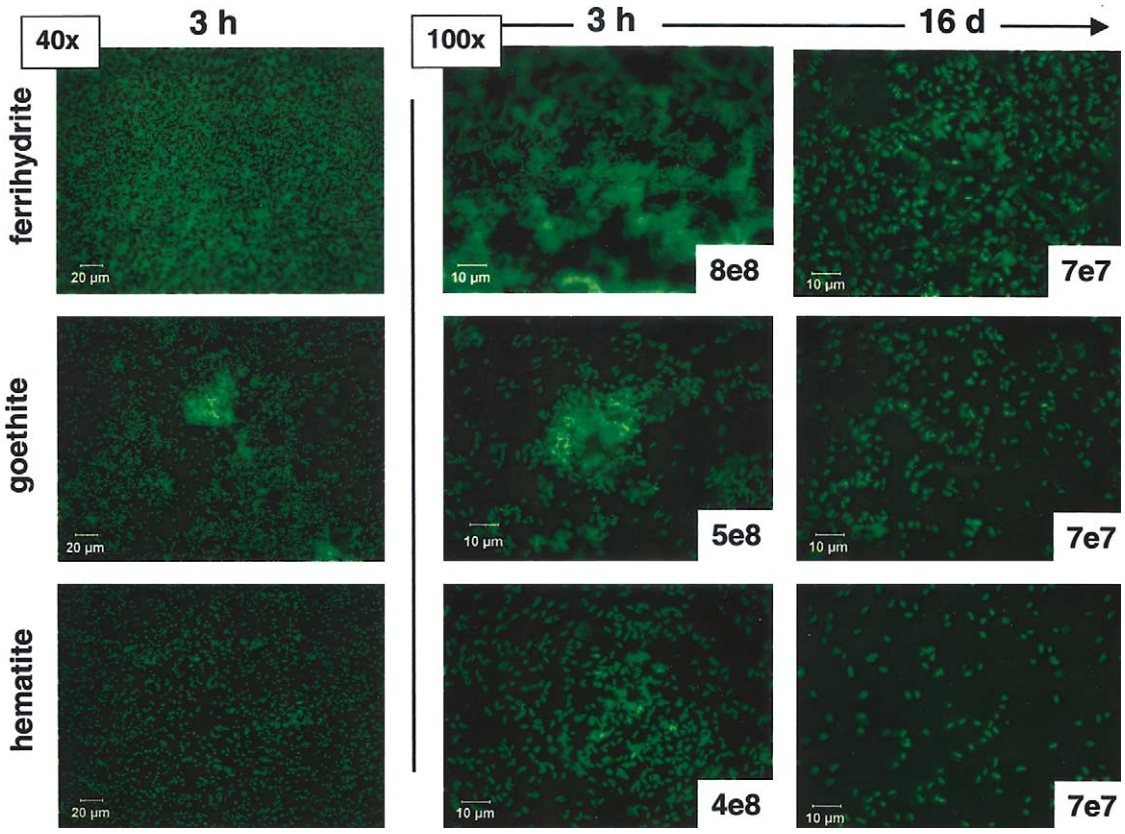

Fig. 8. Epifluorescence images depicting the bacterial coverage of the three Fe (hydr)oxides as a function of time. Time series images were collected at the same scale for direct comparison. Images depicted are representative of the sample as a whole. Significant cell concentration and structure differences were not present among the 1, 4, 16, and 43 d images for each iron oxide. Numbers indicated in the lower right hand corner are the corresponding viable cells after 16 d of reaction determined via serial dilution and plating on tryptic soy agar (3 h) or calculations from steady-state acetate concentrations (16 d).

300 h, acetate and $Fe(II)_{aq}$ concentrations are similar and the rate of Fe(III) reduction declines an order of magnitude from the initial rates to $\sim 10^{-12}$ mol m^{-2} g^{-1} within the 3 iron (hydr)oxide systems (Figs. 1 and 2). Under steady-state conditions, the ratio of effluent ferrous Fe to acetate increases indicating a decline in Fe(II) retention (Fig. 2). For all three (hydr)oxide phases, approximate steady-state concentrations for acetate (40 μM) and $Fe(II)_{aq}$ (150 μM) are in near stoichiometric agreement with the dissimilatory reduction of Fe (reaction [1], 1 acetate:4 $Fe(II)_{aq}$). In fact, the percent of Fe(II) sequestered within the solid-phase in the three oxide systems remains equivalent beyond 16 d of reaction and the concentration of magnetite is constant within the ferrihydrite column (data not shown). The aqueous Fe(II) concentrations therefore are poised at steady-state reduction rates with only minimal continued Fe(II) retention.

Within the 16 d reaction period, a steady-state bacterial population and cell organization on the (hydr)oxide surfaces is obtained. Assuming a maximum value of 6.4×10^6 cells produced per μmol of Fe(II) (see Roden and Zachara, 1996), steady-state $Fe(II)_{aq}$ concentrations (150 μM) yield a maximum cell concentration within each of the three (hydr)oxide columns of $\sim 1 \times 10^8$ cells mL^{-1} ($\sim 7 \times 10^7$ cells g^{-1}). Considering initial cell concentrations of $\sim 5 \times 10^8$ cells g^{-1}, bacterial concentrations decreased an order of magnitude following 16 d of reaction. Acetate concentrations are maintained following 300 h of reaction suggesting that the sustainable (interim) population of iron-reducing bacteria within the iron oxide columns is $\sim 10^7$ cells g^{-1}.

The distribution of cells on the (hydr)oxide surfaces changed dramatically over the course of 16 d converging to a constant and equivalent bacterial population (Fig. 8). Initially, the distribution of microbial cells on the (hydr)oxide surface varies among the three iron (hydr)oxide substrates (Fig. 8). The complexity of the cell distribution decreases from ferrihydrite to goethite to hematite. While ferrihydrite sustains a sinuous network of 3D cell clusters, merely incomplete monolayer coverage is observed for hematite. Cell distribution on goethite is intermediate between that of ferrihydrite and hematite, displaying an incomplete monolayer with random 3D cell clusters (mounds). Upon introduction of advective flow, however, the bacterial distribution on the three (hydr)oxides is equivalent, consisting of an incomplete monolayer and cell numbers appear near equivalent—an observation consistent over columns having 2 different flow rates (25 and 40 cm d^{-1}). The loss of 3D structure upon introduction of advective flow may be a consequence of the mechanism of iron reduction by *S. putrefaciens*. In contrast to *Geobacter* species, *Shewanella* does not require

Table 3. Comparison of Fe(II) production to initial phase disorder.

	Goethite	Hematite
% Fhy component[a]	29	6
Fe(III) as Fhy initially (mmol)	0.34	0.25
Fe(II) production (mmol)		
Within 46 h	0.06	0.04
Within 291 h	0.39	0.34
% Fhy component increase after 16 d[a]	34	34

[a] As mol% Fe determined from EXAFS linear combination fits.

direct contact with the iron (hydr)oxide surface to respire Fe(III) (Lovley and Woodward, 1996; Newman and Kolter, 2000; Nevin and Lovley, 2002). The mechanism of reduction may involve either Fe(III) chelators or electron shuttling compounds (e.g., quinones)—both of which involve the dependence of localization of soluble species. Subsequently, Fe(III) availability due to solute transport under advective flow may impose a limitation on microbial colony thickness.

3.3.3. Role of Site Reactivity in Microbial Reduction

Goethite and hematite phases initially contain a component of ferrihydrite-like disorder corresponding to 0.34 and 0.25 mmol of Fe(III), respectively (Fig. 6; Table 3). Correspondingly, within the first 291 h of reaction, 0.39 and 0.34 mmol of Fe(II) are produced in the goethite and hematite systems, respectively. Thus, the initial disorder (or degree of ′high-energy sites') within the goethite (29%) and hematite (6%) phases may be equated to the amount of Fe(II) generated within the initial pulse of reduction before steady-state reduction (Table 3). Consumption of high energy surface sites may explain the decline in reduction rates within the three (hydr)oxide systems. The initial reduction of higher energy sites followed by slower sustained reduction of lower energy sites has previously been observed (Liu et al., 2001; Rosso et al., 2003). Thus, two stages of Fe(III) reduction are supported here: an early rapid reduction controlled by the initial disorder (reflected in the ferrihydrite-like component) and high energy surface sites followed by a sustained, slower reduction of lower energy sites (Figs. 1 and 2).

An increase in goethite and hematite disorder (ferrihydrite component increases to 34%) transpired following 16 d of reaction and yet a decreased reduction rate is observed (Table 3), contradicting the expected increase in reduction rates with solid-phase disorder. While we confirm the presence of ~1 nm thick hydration (disordered) layers on the surface of reacted goethite and hematite, atomic reorganization into spinel-like (magnetite) domains is not directly observed. Yet, as discussed above, the sequestration of Fe(II) cannot be explained by mere adsorption processes (incomplete 0.5 N HCl extraction compared to 6 N HCl extracts). Declining reduction rates may suggest that the benefit of a surface hydration layer (enhanced disorder similar to ferrihydrite) on microbial reduction is neutralized by localized magnetite nucleation sites (nano-scale spinel domains) within the hydration layers (resulting in localized low energy surface sites). As a consequence, lower energy sites become the predominant available sites for reduction since magnetite nucleation would initiate and be expected to consume higher energy sites. In addition, sequestration of Fe(III) within magnetite, which is not a viable electron acceptor at circumneutral pH, reduces the bioavailablility of Fe(III) for microbial reduction (Kostka and Nealson, 1995). Alternatively, delocalized electron density within the bulk phase may alter surface reactivity and the reducing capacity of the solid-phase. Thus, microbial reduction capacity of all three (hydr)oxide phases may be poised by electron delocalization and/or magnetite precipitation leading to a slower, steady-state Fe(III) reduction rate.

In addition to declines in microbial reduction rates and Fe(II) retention, changes in surface reactivity may also influence cell migration and transport. Besides the observed changes in cell distribution and associations, epifluorescence images also reveal a decrease in overall cell numbers as a function of (hydr)oxide substrate and time. Over the 16 d reaction period, a substantial concentration of viable cells ($>10^6$ CFU) is eluted from all three columns (determined via serial dilution plating). The loss of viable cells under advective flow has previously been attributed to migration of daughter cells before attachment (Roden et al., 2000). As surface area and available active sites decrease on the (hydr)oxide substrates, daughter cells may undergo an enhanced migration and subsequent elution from the column. Similarly, substrate limitation, as surface sites are consumed via microbial reduction or magnetite nucleation, may induce detachment of viable cells. Cells may detach from areas where growth factors may be depleted to emigrate to regions more amenable to growth. The extent of reattachment, however, may be a function of advective flow and physiologic status (Lawrence et al., 1995). As such, viable cell loss in the three columns may be ultimately controlled by the initial extent of microbial reduction and secondary mineralization and hence subsequent availability of surface area and reactive surface sites.

3.4. Reproducibility

As aforementioned the reproducibility of the results obtained in the 16 d reacted column experiments was investigated by performing additional column studies varying in the initial Fe(III) content and flow rate (time series columns). Microbial reduction rates, extent of Fe(III) reduction, and bacterial populations are equivalent between the 16 d reacted and time series columns for each (hydr)oxide. Additionally, the aqueous chemistry, solid-phase transformations, and microbial dynamics within the ferrihydrite column are equivalent to results obtained previously (Hansel et al., 2003a).

4. CONCLUSIONS AND IMPLICATIONS

Although overall surface area normalized reduction rates are equivalent among 2-line ferrihydrite, goethite, and hematite, the extent of Fe(III) reduction and mechanisms of Fe(II) retention differs among the three systems. While the fate of Fe(II) within all three systems may involve the nucleation and sequestration of Fe(II) within magnetite, the degree of conversion varies. The initial reduction of ferrihydrite results in a greater degree of Fe(II) generation and accumulation (as a magnetite phase) compared to goethite and hematite. Goethite and hematite illustrate a similar control on Fe(II) dynamics, where Fe(II)

primarily remains in the aqueous phase and is eluted from the system. A smaller degree of Fe(II) retention results in Fe(II) adsorption and/or minor (<1%) magnetite precipitation on the goethite and hematite surfaces. Iron(II) sequestration ranges from magnetite precipitation and crystal growth on ferrihydrite to possible localized spinel-like (magnetite) domains within surface hydrated layers (~1 nm thick) on goethite and hematite. The lower solubility of goethite and hematite relative to ferrihydrite resulting in lower $Fe(III)_{aq}$ and bacterially-generated $Fe(II)_{aq}$ concentrations may hinder magnetite precipitation beyond mere surface reorganization into nanometer-sized, spinel-like domains. Recent evidence, however, suggests that Fe(II) may not be preserved upon abiotic reaction with iron (hydr)oxides (Scherer, M., personal communication) and instead electron delocalization may occur within the solid-phase. Changes in electron density may therefore alter surface reactivity and subsequent reduction potential.

Nevertheless, despite the differences in initial reduction and retention, the subsequent rate of Fe(II) generation reaches an equivalent steady-state for the three Fe (hydr)oxides, in which similar aqueous ferrous iron concentrations, bacterial populations, and microbial Fe(III) reduction rates are noted. The decline in microbial reduction is, most likely, due to preferential consumption of higher energy surface sites and changes in surface energy (reactivity) via microbial reduction, magnetite nucleation, and electron transduction. The persistence of lower energy sites or diminished surface passivation allows for slower, sustained reduction and a subsequent decline in Fe(II) retention. As such, sustained microbial reduction of ferrihydrite, goethite, and hematite is largely controlled by changes in surface reactivity (energy). The secondary Fe(II) retention mechanism, in part, governs the availability of reactive sites and is equivalent for the various (hydr)oxides studied regardless of structural order and surface area. Initial reduction rates for the various iron (hydr)oxides therefore may not be representative of sustainable reduction resulting in an inaccurate portrayal of either the extent or sustained rate of reduction and ultimate fate of Fe(II). Similarly, given the transient nature of reactive sites on ferrihydrite, microbial reduction and colonization may not differ substantially from that of goethite and hematite. Given the greater abundance of more crystalline iron (hydr)oxides in the environment, microbial reduction of phases such as goethite and hematite may impart an equivalent or potentially greater impact on sustained, long-term Fe(II) generation, retention, and associated biogeochemical cycles as that of ferrihydrite.

Acknowledgments—We are very grateful to Alice Dohnalkova for her time and assistance in TEM analysis. TEM was performed in the Environmental Molecular Sciences Laboratory, a national scientific user facility sponsored by the Department of Energy's Office of Biologic and Environmental Research (OBER), located at Pacific Northwest National Laboratory. We also thank Dr. Jillian Banfield's research group at UC Berkeley, specifically John Moreau and Brett Baker, for assistance with the FISH analysis and for supplying the EUB338 FISH probes. This research was funded by the Natural and Accelerated Bioremediation Research (NABIR) program, Biologic and Environmental Research (BER), U.S. Department of Energy (grant DE-FG03-00ER63029). X-ray absorption spectroscopy was carried out at the Stanford Synchrotron Radiation Laboratory, a national user facility operated by Stanford University on behalf of the U.S. Department of Energy, Office of Basic Energy Sciences. The SSRL Structural Molecular Biology Program is supported by the Department of Energy, Office of Biologic and Environmental Research, and by the National Institutes of Health, National Center for Research Resources, Biomedical Technology Program. The authors are also grateful to Jim Fredrickson, Bill Burgos, and Associate Editor Jeremy Fein for their helpful comments and suggestions, which substantially strengthened the manuscript.

Associate editor: J. B. Fein

REFERENCES

Allison J. D., Brown D. S., and Nova-Gradac K. J. (1990) *MINTEQA2/PRODEFA2, a Geochemical Assessment Model for Environmental Systems: Version 3.0 User's Manual*. U.S. EPA.

Baes C. F. and Mesmer R. E. (1976) *The Hydrolysis of Cations*. Wiley.

Balch W. E., Fox G. E., Magrum L. J., Woese C. R., and Wolfe R. S. (1979) Methanogens: Re-evaluation of a unique biological group. *Microb. Rev.* **43,** 260–296.

Benner S. G., Hansel C. M., Wielinga B. W., Barber T. M., and Fendorf S. (2002) Reductive dissolution and biomineralization of iron hydroxide under dynamic flow conditions. *Environ. Sci. Technol.* **36,** 1705–1711.

Bond P. L. and Banfield J. F. (2001) Design and performance of rRNA targeted oligonucleotide probes for in situ detection and phylogenetic identification of microorganisms inhabiting acid mine drainage environments. *Microb. Ecol.* **41,** 149–161.

Caccavo F., Jr., Blakemore R. P., and Lovley D. R. (1992) A hydrogen-oxidizing, Fe(III)-reducing microorganism from the Great Bay Estuary, New Hampshire. *Appl. Environ. Microb.* **58,** 3211–3216.

Caccavo F., Jr., Lonergan D. J., Lovley D. R., Davis M., Stolz J. F., and McInerney M. J. (1994) *Geobacter sulfurreducens* sp.nov., a hydrogen- and acetate-oxidizing dissimilatory metal-reducing microorganism. *Appl. Environ. Microb.* **60,** 3752–3759.

Childers S. E. and Lovley D. R. (2001) Differences in Fe(III) reduction in the hyperthermophilic archaeon. Pyrobaculum islandicum, versus mesophilic Fe(III)-reducing bacteria. *FEMS Microb. Let.* **195,** 253–258.

Childers S. E., Ciufo S., and Lovley D. R. (2002) Geobacter metallireducens accesses insoluble Fe(III) oxide by chemotaxis. *Nature* **416,** 767–769.

Condon N. G., Leibsle F. M., Lennie A. R., Murray P. W., Parker T. M., Vaughan D. J., and Thornton G. (1998) Scanning tunneling microscopy studies of a-Fe_2O_3(0001). *Surf. Sci.* **397,** 278–287.

Cooper D. G., Picardal F., Rivera J., and Talbot C. (2000) Zinc immoblization and magnetite formation via ferric oxide reduction by *Shewanella putrefaciens* 200. *Geochim. Cosmochim. Acta* **34,** 100–106.

Coppi M. V., Leang C., Sandler S. J., and Lovley D. R. (2001) Development of a genetic system for *Geobacter sulfurreducens*. *Appl. Environ. Microb.* **67,** 3180–3187.

Cornell R. M. (1988) The influence of some divalent cations on the transformation of ferrihydrite into more crystalline products. *Clay Mineral.* **23,** 329–332.

Cornell R. M. and Schwertmann U. (1996) *The Iron Oxides: Structure, Properties, Reactions, Occurrence and Uses*. VCH.

Coughlin B. R. and Stone A. T. (1995) Nonreversible adsorption of divalent metal ions (Mn^{II}, Co^{II}, Ni^{II}, Cu^{II}, and Pb^{II}) onto goethite: Effects of acidification, Fe^{II} addition, and picolinic acid addition. *Environ. Sci. Technol.* **29,** 2445–2455.

DiChristina T. J. and DeLong E. F. (1994) Isolation of anaerobic respiratory mutants of *Shewanella putrefaciens* and genetic analysis of mutants deficient in anaerobic growth on Fe^{3+}. *J. Bacteriol.* **176,** 1468–1474.

DiChristina T. J., Moore C. M., and Haller C. A. (2002) Dissimilatory Fe(III) and Mn(IV) reduction by. Shewanella putrefaciens requires *ferE*, a homolog of the pulE (*gspE*) type II protein secretion gene. *J. Bacteriol.* **184,** 142–151.

Fendorf S., Wielinga B. W., and Hansel C. M. (2000) Chromium transformations in natural environments: The role of biological and abiological processes in chromium(VI) reduction. *Int. Geol.* **42,** 691–701.

Fredrickson J. K., Zachara J. M., Kennedy D. W., Dong H., Onstott T. C., Hinman N. W., and Li S.-M. (1998) Biogenic iron mineralization accompanying the dissimilatory reduction of hydrous ferric oxide by a groundwater bacterium. *Geochim. Cosmochim. Acta* **62,** 3239–3257.

Fredrickson J. K., Kota S., Kukkadapu R. K., Liu C. X., and Zachara J. M. (2003) Inifluence of electron donor/acceptor concentrations on hydrous ferric oxide (HFO) bioreduction. *Biodegradation* **14,** 91–103.

George G. N. (1993) EXAFSPAK. Stanford Synchrotron Radiation Laboratory.

Glasauer S., Weidler P. G., Langley S., and Beveridge T. J. (2003) Controls on. Fe reduction and mineral formation by a subsurface bacterium. *Geochim. Cosmochim. Acta* **67,** 1277–1288.

Gorby Y. A. and Lovley D. R. (1991) Electron transport in the dissimilatory iron reducer, GS-15. *Appl. Environ. Microb.* **57,** 867–870.

Hansel C. M., Benner S. G., Neiss J., Dohnalkova A., Kukkadapu R. K., and Fendorf S. (2003a) Secondary mineralization pathways induced by dissimilatory iron reduction of ferrihydrite under advective flow. *Geochim. Cosmochim. Acta* **67,** 2977–2992.

Hansel C. M., Wielinga B. W., and Fendorf S. (2003b) Structural and compositional evolution of Cr/Fe solids after indirect chromate reduction by dissimilatory iron-reducing bacteria. *Geochim. Cosmochim. Acta* **67,** 401–412.

Jeon B. H., Dempsey B. A., Burgos W. D., and Royer R. A. (2001) Reactions of ferrous iron with hematite. Colloids Surf. *A Physicochem. Eng. Aspects* **191,** 41–55.

Kostka J. E. and Nealson K. H. (1995) Dissolution and reduction of magnetite by bacteria. *Environ. Sci. Technol.* **29,** 2535–2540.

Langmuir D. (1969) The Gibbs free energies of substrates in the system Fe-O_2-H_2O-CO_2 at 25C. Prof. Paper. 650-B, B180– B184. U.S. Geol. Surv.

Lawrence J. R., Korber D. R., Wolfaardt G. M., and Caldwell D. E. (1995) Behavioral strategies of surface-colonizing bacteria. *Adv. Microb. Ecol.* **14,** 1–75.

Leang C., Coppi M. V., and Lovley D. R. (2003) OmcB, a c-type polyheme cytochrome, involved in Fe(III) reduction in *Geobacter sulfurreducens*. *J. Bacteriol.* **185,** 2096–2103.

Liu P., Kendelewicz T., Brown G. E., Jr., Nelson E. J., and Chambers S. A. (1998) Reaction of water vapor with a-Al_2O_3(0001) and a-Fe_2O_3(0001) surfaces: Synchrotron X-ray photoemission studies and thermodynamic calculations. *Surf. Sci.* **417,** 53–65.

Liu C., Kota S., Zachara J. M., Fredrickson J. K., and Brinkman C. K. (2001) Kinetic analysis of the bacterial reduction of goethite. *Environ. Sci. Technol.* **35,** 2482–2490.

Lloyd J. R., Leang C., Hodges-Myerson A. L., Coppi M. V., Cuifo S., Methe B., Sandler S. J., and Lovley D. R. (2003) Biochemical and genetic characterization of PpcA, a periplasmic c-type cytochrome in *Geobacter sulfurreducens*. *Biochem. J.* **369,** 153–161.

Lovley D. R. (1991) Dissimilatory Fe(III) and Mn(IV) reduction. *Microb. Rev.* **55,** 259–287.

Lovley D. R. and Phillips E. J. P. (1986) Availability of ferric iron for microbial reduction in bottom sediments of the freshwater tidal Potomac River. *Appl. Environ. Microb.* **52,** 751–757.

Lovley D. R. and Phillips E. J. P. (1988) Novel mode of microbial energy metabolism: Organic carbon oxidation coupled to dissimilatory reduction of iron or manganese. *Appl. Environ. Microb.* **54,** 1472–1480.

Lovley D. R., Phillips E. J. P., and Lonergan D. J. (1991) Enzymatic versus nonenzymatic mechanisms for Fe(III) reduction in aquatic sediments. *Environ. Sci. Technol.* **25,** 1062–1067.

Lovley D. R. and Woodward J. C. (1996) Mechanisms for chelator stimulation of microbial Fe(III)-oxide reduction. *Chem. Geol.* **132,** 19–24.

Magnuson T. S., Hodges-Myerson A. L., and Lovley D. R. (2000) Characterization of a membrane-bound NADH-dependent Fe^{3+} reductase from the dissimilatory Fe^{3+}-reducing bacterium *Geobacter sulfurreducens*. *FEMS Microb. Lett.* **185,** 205–211.

Myers J. M. and Myers C. R. (1998) Isolation and sequence of *omcA*, a gene encoding a decaheme outer membrane cytochrome *c* of *Shewanella putrefaciens* MR-1, and detection of *omcA* homologs in other strains of *S. putrefaciens*. *Biochim. Biophys. Acta* **1373,** 237–251.

Nealson K. H. and Saffarini D. (1994) Iron and manganese in anaerobic respiration: Environmental significance, physiology, and regulation. *Annu. Rev. Microbiol.* **48,** 311–343.

Nevin K. P. and Lovley D. R. (2000) Lack of production of electron-shuttling compounds or solubilization of Fe(III) during reduction of insoluble Fe(III) oxide by *Geobacter metallireducens*. *Appl. Environ. Microb.* **66,** 2248–2251.

Nevin K. P. and Lovley D. R. (2002) Mechanisms of Fe(III) oxide reduction in sedimentary environments. *Geomicrob. J.* **19,** 141–159.

Newman D. K. and Kolter R. (2000) A role for excreted quinones in extracellular electron transfer. *Nature* **405,** 94–97.

Phillips E. J. P., Lovley D. R., and Roden E. E. (1993) Composition of non-microbially reducible Fe(III) in aquatic sediments. *Appl. Environ. Microb.* **59,** 2727–2729.

Roden E. E. (2003) Fe(III) oxide reactivity toward biological versus chemical reduction. *Environ. Sci. Technol.* **37,** 1319–1324.

Roden E. E. and Zachara J. M. (1996) Microbial reduction of crystalline iron(III) oxides: Influence of oxide surface area and potential for cell growth. *Environ. Sci. Technol.* **30,** 1618–1628.

Roden E. E. and Urrutia M. M. (1999) Ferrous iron removal promotes microbial reduction of crystalline iron(III) oxides. *Environ. Sci. Technol.* **33,** 1847–1853.

Roden E. E., Urrutia M. M., and Mann C. J. (2000) Bacterial reductive dissolution of crystalline Fe(III) oxide in continuous-flow column reactors. *Appl. Environ. Microb.* **66,** 1062–1065.

Roden E. E. and Urrutia M. M. (2002) Influence of biogenic Fe(II) on bacterial crystalline Fe(III) oxide reduction. *Geomicrob. J.* **19,** 209–251.

Rosso K. M., Zachara J. M., Fredrickson J. K., Gorby Y. A., and Smith S. C. (2003) Nonlocal bacterial electron transfer to hematite surfaces. *Geochim. Cosmochim. Acta* **67,** 1081–1087.

Royer R. A., Burgos W. D., Fisher A. S., Unz R. F., and Dempsey B. A. (2002) Enhancement of biological reduction of hematite by electron shuttling and Fe(II) complexation. *Environ. Sci. Technol* **36,** 1939–1946.

Schwertmann U. and Cornell R. M. (2000) *Iron Oxides in the Laboratory: Preparation and Characterization*. Wiley-VCH.

Stookey L. L. (1970) Ferrozine—A new spectrophotometric reagent for iron. *Anal. Chem.* **42,** 779–781.

Tamura H., Goto K., Yotsuyanagi T., and Nagayama M. (1974) Spectrophotometric determination of iron(II) with 1,10-phenanthroline in the presence of large amounts of iron(III). *Talanta* **21,** 314–318.

Thompson D. K., Beliaev A. S., Giometti C. S., Tollaksen S. L., Khare T., Lies D. P., Nealson K. H., Lim H., Yates J., III, Brandt C. C., Tiedje J. M., and Zhou J. (2002) Transcriptional and proteomic analysis of a ferric uptake regulator (Fur) mutant of *Shewanella oneidensis*: Possible involvement of Fur in energy metabolism, transcriptional regulation, and oxidative stress. *Appl. Environ. Microb.* **68,** 881–892.

Tronc E., Belleville P., Jolivet J. P., and Livage J. (1992) Transformation of ferric hydroxide into spinel by Fe(II) adsorption. *Langmuir* **8,** 313–319.

Urrutia M. M., Roden E. E., and Zachara J. M. (1999) Influence of aqueous and solid-phase Fe(II) complexants on microbial reduction of crystalline iron(III) oxides. *Environ. Sci. Technol.* **33,** 4022–4028.

Wielinga B., Mizuba M. M., Hansel C. M., and Fendorf S. (2001) Iron promoted reduction of chromate by dissimilatory iron-reducing bacteria. *Environ. Sci. Technol.* **35,** 522–527.

Zachara J. M., Kukkadapu R. K., Fredrickson J. K., Gorby Y. A., and Smith S. C. (2002) Biomineralization of poorly crystalline Fe(III) oxides by dissimilatory metal reducing bacteria (DMRB). *Geomicrob. J.* **19,** 179–207.